Compact Pulsed Power Sources

Jon R. Mayes and William J. Carey
Applied Physical Electronics, L.C.

ABSTRACT

Marx generators have been traditionally relegated as pulse-charging supplies for a variety of applications including the generation of High Power Microwaves, or RF energy. Compact models have served as suitable trigger generators for larger systems. However, recent work has demonstrated the compact Marx generators for directly generating RF energy.

This paper discusses two compact Marx generators developed for RF applications. General performance characteristics for each generator are discussed, as well as efforts to minimize the temporal jitter of these systems so as to make them viable sources for radar transmitters. The Gatling Marx generator is presented as a multiple generator RF source for weapons and radar transmitters. Finally, the generation of RF and microwave energy is discussed.

INTRODUCTION

Marx generators have been traditionally relegated as pulse-charging supplies for a variety of applications including the generation of High Power Microwaves, or RF energy. Typically, these systems are large in volume and mass.

Compact versions of the Marx generator have been employed for many years as trigger generators for larger systems. These generators are typically designed with pulse characteristics of more than 200 kV in peak voltage, 3 – 4 ns rise times, 1 – 3 ns rms jitter and pulse widths of 10's of ns. The usefulness of these generators does not extend much beyond the role of trigger source since its highest frequency component is only 950 MHz.

However, recent efforts[1] with compact Marx generators have brought faster rise times, higher peak voltages, and extremely low jitter values, making them viable candidates for compact Ultra Wideband (UWB) sources for both single and multiple generator systems.

This paper discusses the generators under development by Applied Physical Electronics, L.C., or APELC, for both single generator and multiple generator systems. These generators are designed for performance with the primary emphasis on the generation of high power RF. Once the generator systems have been presented, applications in the form of RF generation will be discussed and include impulse radiating antennas and the Backward Wave Oscillator, or BWO.

THE WAVE ERECTION MARX GENERATOR

The most efficient, compact and economical method of generating a repetitive, large magnitude, electromagnetic impulse is the wave erection of a spark gap-switched Marx circuit. Wave erection is necessary to obtain the fast voltage rise times from the Marx circuit that generates the ultra-wideband of frequencies necessary for high resolution radar or the interdiction of flight controls and computer memories for electronic warfare.

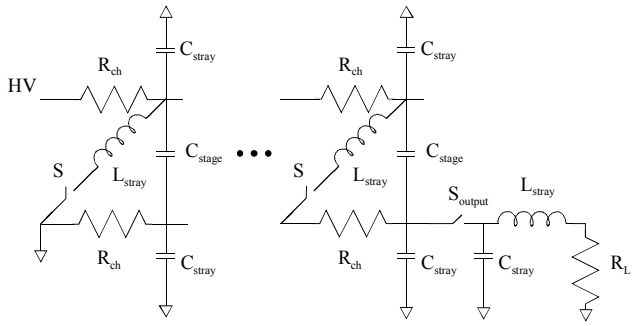

Figure 1. The Wave-Erection Marx Generator.

The conventional Marx circuit, illustrated in Figure 1, charges capacitors in parallel through resistors, and then switches the capacitors, using spark gap switches, in series to add the individual capacitor voltages at the output terminals. This approach multiplies the charge voltage by the number of stages to yield a large output voltage. Proper design of the stray capacitance and the inter-stage capacitance, in concert with coupling the spark gaps via ultra-violet energy, results in a sub-ns rise time for output voltages of several hundred kV at moderate per pulse energies.

THE APELC MARX GENERATORS

APELC has primarily worked toward the development of two generators; the impulse generator and the moderate pulse generator, which are discussed in the following sections. The impulse generator is fundamentally designed for direct RF generation, delivering pulses with a frequency spectrum ranging from a few GHz down to 10's of MHz. As a result, Ultra Wide Band (UWB) antennas, such as loops and TEM horns may be driven directly by the generator. The moderate pulse generator is specifically designed for driving the cathode of a BWO.

THE IMPULSE MARX GENERATOR

APELC's impulse generators are based on very compact geometries, delivering low amounts of energy in just a few nanoseconds. These generators may be battery-powered for autonomous applications.

The generator used for this discussion was a 17-stage Marx with a 30 kV charging voltage. As shown in Figure 2, the generator delivers a short impulse that is approximately 1 ns, full width half maximum (FWHM), with a rise time of 200 ps and a voltage efficiency of 65%. The impulse peaks at about 360 kV and is followed by a longer plateau of approximately 125 kV, which decays to zero within 14 ns. The peak power of the impulse is approximately 2.6 GW.

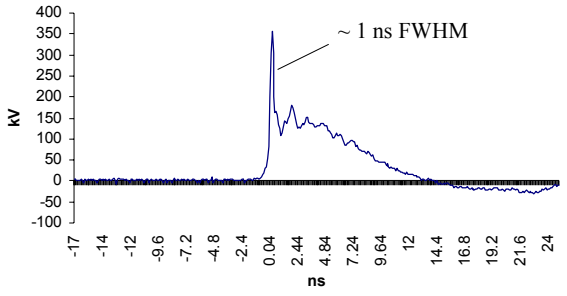

Figure 2. Output waveform from the Impulse Marx generator.

Physically, this generator is encased in a 76 mm diameter tube of length of 1 m. At approximately 15 lb, this generator is well suited as a man portable system.

THE MODERATE PULSE MARX GENERATOR

APELC's narrowband source generator is also based on the wave-erection principle. This generator is a 13-stage, 3 nF capacitance per stage design sourced by a 40 kV supply voltage. The Marx circuit occupies approximately 60% of the cylindrical housing structure (127 mm diameter, 1 m length), allowing additional volume for future pulse-shaping circuitry

As shown in Figure 3, the output waveform is characterized by a 3 ns rise time and a peak voltage of 270 kV, or 1.5 GW into the 50 Ohm load, and delivers 32 J in approximately 20 ns, FWHM.

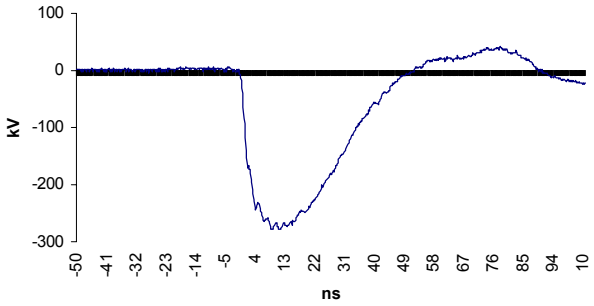

Figure 3. The narrowband generator source output.

SUB-NANOSECOND JITTER OPERATION

Low temporal jitter of the impulse Marx generator may be required for multi-source applications or timing applications.[2] For the Marx generator to be a viable candidate for phased array systems, the jitter must be reduced to a small fraction of its pulse width, 200 ps in these case of the 1 ns impulse. Similar results must also be achieved for multiple pulse addition circuits such as Gatling-styled systems and bistatic radar systems.

Achieving low jitter with the wave erection Marx generators is primarily accomplished with reducing the jitter of the trigger gap, which is the first gap of the generator. A brief discussion triggering spark gaps is presented in the following section.

SPARK GAP TRIGGERING

There are three basic triggered spark gap types including the trigatron, the laser-triggered and the field distortion[3]. The trigatron gap of Figure 4(a) is a three electrode gap with the voltage held off between the anode and cathode. The third electrode, or the trigger pin, is placed within the cathode electrode such that initial closure of the spark gap begins with a breakdown between the trigger pin and the cathode. This initial breakdown generates a plasma in the high field region between the anode and cathode and ultimately leads to the breakdown of the main gap. These systems are very easily fabricated and simply require a high voltage pulse for triggering. Unfortunately, these systems result in high jitter values due to the fact that two breakdown events are required for switch closure.

The laser-triggered spark gap of Figure 4(b) relies on optical energy to vaporize a portion of the metal electrode. The hot metal vapor emits ultraviolet energy, which then produces free electrons at the electrode surface. Furthermore, the laser also pre-ionizes the path back to the opposite electrode. The electric field then heats the streamer to reduce the resistance and leads to closure of the spark gap. These systems are

more difficult to fabricate and require large pulsed laser systems for triggering. However, the lowest spark gap jitter recorded came from a laser-triggered spark gap and resulted in a jitter of 50 ps.

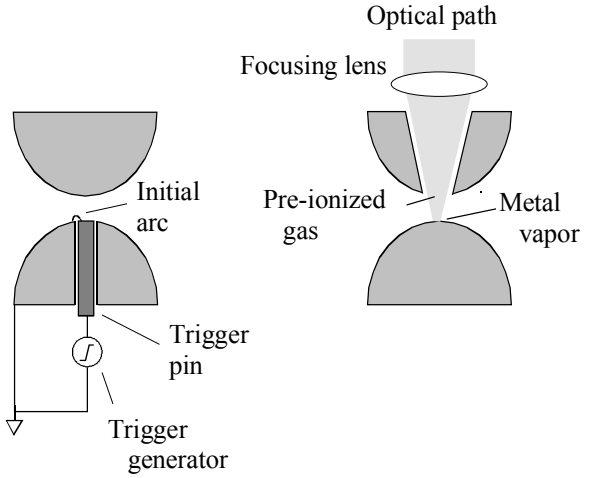

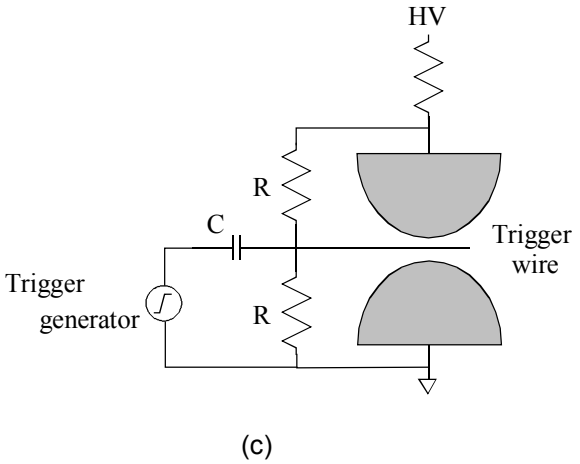

Figure 4. Triggered spark gaps. (a) the trigatron, (b) the laser triggered, and (c) field distortion triggered gaps.

The third spark gap-triggering method, the field distortion gap of Figure 4(c), a dc-biased pin is placed between the anode and cathode such that the electric field is not disturbed. Gap closure is initiated when a negative pulse is delivered to the trigger pin and results in a highly distorted electric field between the main electrodes. The field distortion spark gap is ideal for low jitter applications, since the two breakdown events occur simultaneously.

The closure of a spark gap is a statistical process. However, the breakdown process is sequential. Consider a spark gap that is closed by over-volting. Initially, the spark gap voltage is set just below the statistical breakdown level, VSB, as shown in Figure 5. The time for the breakdown process to occur is dependent on four events: (1) the statistical time delay for the appearance of a free electron, tsd, which may be reduced to zero with the application of a UV source; (2) the streamer formation time, tsf, which is inversely proportion to the electric field; (3) the channel heating time, tch, which is also inversely proportional to the electric field; and (4), the trigger pulse rise time, tr.

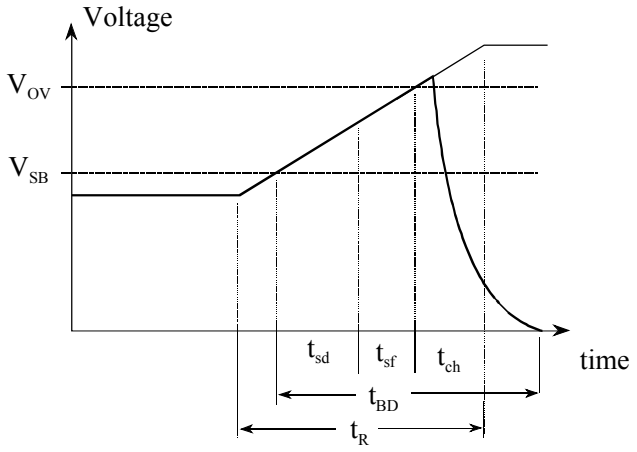

Figure 5. The spark gap breakdown sequence.

Reduction in temporal jitter for the field distortion gap is primarily dependent on three parameters: UV illumination, a fast-rising trigger pulse (10 kV/ns), and a trigger voltage approximately equal in magnitude to the charging voltage. Achieving a spark gap jitter of less than 200 ps will require an extremely fast trigger source.

TRIGGERING THE FIELD DISTORTION SPARK GAP

The method chosen for triggering the field distortion spark gap involves replacing the DC blocking capacitor shown in Figure 4 (c) with a short coaxial line, as illustrated in Figure 6. This coaxial line, referred to as the trigger line, is DC biased to ½ the charging voltage of the spark gap. Note that the trigger switch must hold off the DC bias voltage.

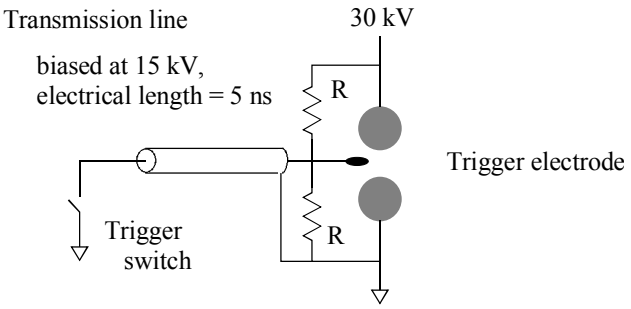

Figure 6. Initial state of the field distortion spark gap.

Upon closure of the trigger switch, a reflected pulse of -½ the spark gap charge voltage and of a length that is twice that of the charged transmission line propagates toward the spark gap, as shown in Figure 7. Arriving at the end of the trigger pin, the pulse doubles in magnitude, resulting in a potential of minus one-half the

charge voltage. This results in a highly distorted field between the electrodes due to the presence of the small pin at the negative potential.

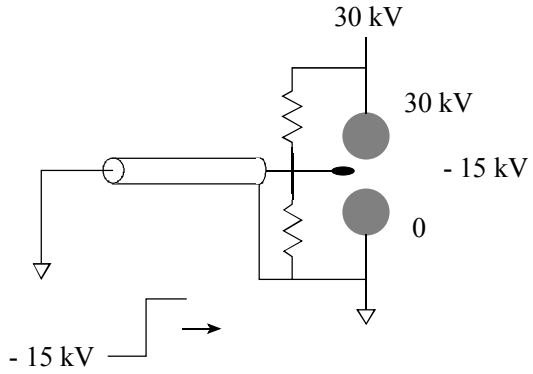

Figure 7. Triggering of the field distortion spark gap.

TRIGGERING, PRACTICE AND MEASUREMENT

Gas switches, krytrons and thyratrons, offer mature technologies for triggering the Marx generator. Although these devices offer high voltage and high current capabilities, they are inherently high in jitter (several ns) and are typically slow devices, with rise times ranging from a few ns to 10's of ns. As shown in Figure 8, a krytron stack is used to trigger the Marx generator. This design is fabricated for extremely low inductance, resulting in a closure time of 1.5 ns.

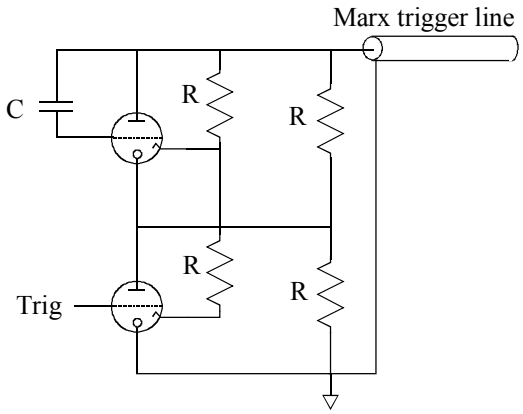

Figure 8. Marx generator trigger circuit.

The described trigger circuit is used with the APELC impulse generator. The generator was resistively charged with a 30 kV power supply, and was fitted with the field distortion trigger gap, as described in Figure 6. The output of the Marx was connected to a long section of RG-220 coaxial cable that was fitted with an uncalibrated capacitive voltage divider. A second capacitive voltage divider was placed on the trigger line, just outside the generator.

As shown in Figure 9, measurements of the Marx generator are limited the generator itself. The capacitive probe on the trigger line simply acts as a trigger signal for the SCD5000, while the output capacitive probe monitors the generator's output. In this manner, the temporal response of the generator was isolated from the trigger system.

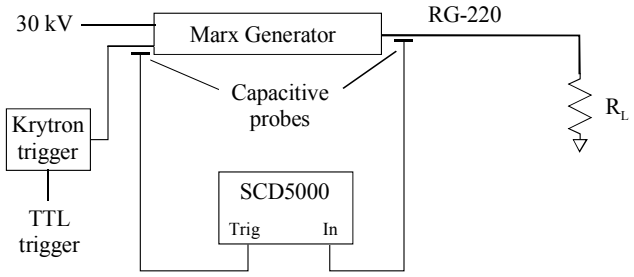

Figure 9. Experimental arrangement.

Three samples of the system were made with each being unique in the length of the trigger cable. Sample 1, shown in Figure 10, used a 5 ns trigger cable and resulted in a pulse spread of the 540 ps, with a standard deviation of 114 ps. Sample 2 used a trigger line of 30 ns. Figure 11 shows the resulting set of waveforms, with an apparent increase in rms jitter, approximately 196 ps, and a spread of 620 ps. Finally, the trigger line length for sample 3 was chosen at 60 ns. Figure 12 reveals the sample waveforms. The spread was approximately 1.18 ns, with a jitter of 285 ps. The effect of dispersion become obvious from these measurements.

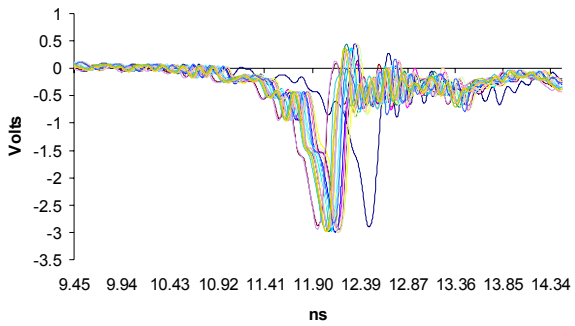

Figure 10. Output samples with a 5 ns trigger line.

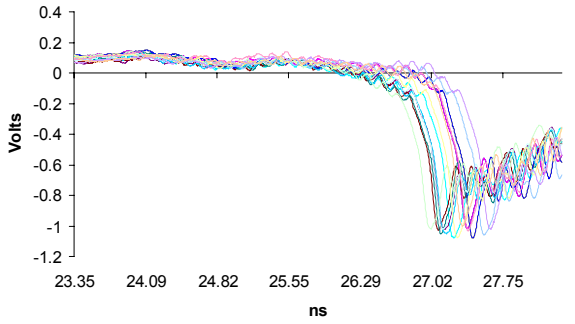

Figure 11. Output samples with a 30 ns trigger line.

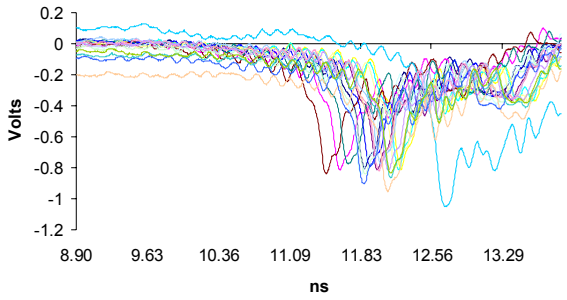

Figure 12. Output samples with a 60 ns trigger line.

THE GATLING MARX GENERATOR SYSTEM

The Gatling Marx generator system is fundamentally designed for delivering high voltage pulses at extremely high repetition rates. For continuous operation repetition rates of 50 kHz is achievable, with a 50 generator system. However, in the burst mode, in which the time separation between each pulse is minimized, repetition rates in excess of 50 MHz are achievable. The following sections discuss the operation of this system.

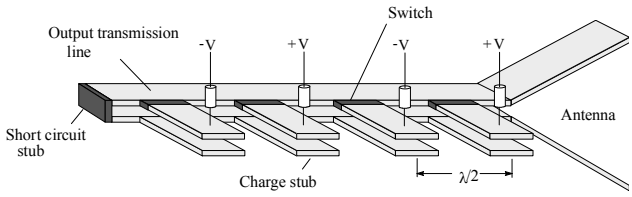

Figure 13. The Injection Wave Generator.

THE GALTING THEORY

The Injection Wave Generator[4] (IWG) uses multiple parallel energy sources to produce an RF burst into a single transmission line directly from DC, as shown in Figure 13. Work on the IWG has been limited to a photoconductive switch-based system.

An illustration of pulse generation and pulse propagation is shown in Figure 14. At each injection point, two pulses are generated immediately following switch closure: a forward wave moving toward the load, and a rearward wave moving toward the short circuit stub at the opposite end of the line, as shown in Figure 13 a). The rearward moving wave is negatively reflected by the short circuit stub and follows the forward moving wave to the matched load after a time delay defined by the two-way transit time from the switch to the short as illustrated in Figure 13 b).

In essence, each charge section delivers a full cycle of energy. In general, however, the two halves of the cycle are separated by the two-way transit time. Only the injection point closest to the short-circuit stub produces a cohesive cycle of energy. Subsequent charge sections simply add pulses to the front of the forward moving wave and to the end of the rearward moving wave.

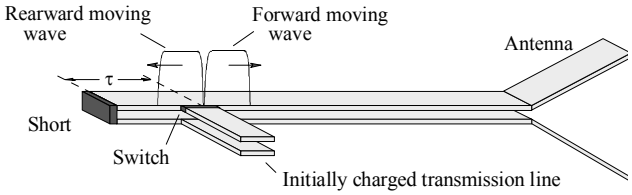

(a)

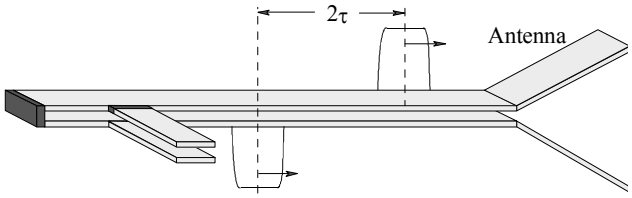

(b)

Figure 14. Propagation and spatial dependence of the injected waves, (a) launched waves, (b) resulting propagation.

THE EXPERIMENTAL GATLING SYSTEM

The Gatling Marx Generator system takes the IWG concept and replaces the transmission line stubs with wave erection Marx generators. Each generator is essentially isolated from the common transmission line with magnetic material, as illustrated in Figure 15. Also, all of the injection points are located at a common point on the output transmission line.

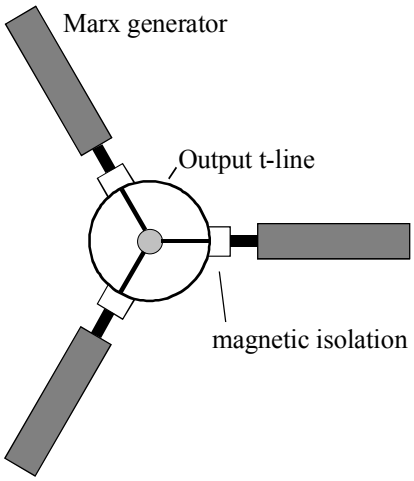

Figure 15. Generator interconnection with output transmission line.

Operationally, when the system is fired, each generator delivers a pulse onto the common transmission line. As described in the Injection Wave Generator section of this paper, the forward-moving wave proceeds directly to the load and the rearward-moving wave is launched toward the short of the common transmission line. However, upon reflection, most of the energy of the rearward-moving wave is absorbed back into the magnetic material, resetting the ferrite to its original state.

The final experimental arrangement is shown in Figure 16. This figure shows two generators connected to the common output transmission line at a common launching point (generator 3 is not shown). All three of the generators are triggered by a single trigger circuit, which is based on a krytron-stack configuration. The coaxial lines connecting each of the generators to the trigger circuit are unique in length, thus offering delays between the pulses delivered to the output line. A capacitive voltage divider is located at the output of one of the Marx generators and is used as a trigger signal for the SCD5000. A second capacitive probe is placed at the output of the Gatling system to monitor the generated signal.

Since the custom output transmission line may be characterized as having a large diameter, a coaxial taper guides the Gatling signal onto a long section of RG-220.

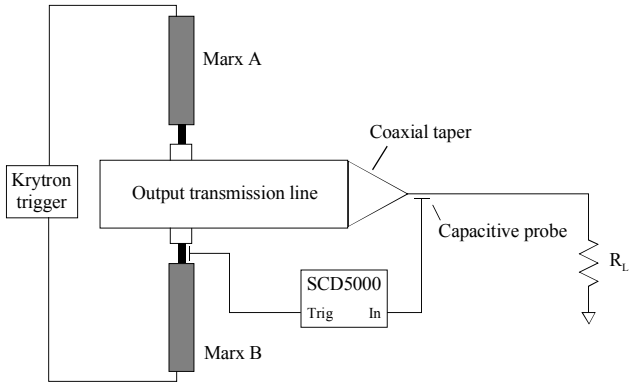

Figure 16. The Gatling system experimental arrangement.

Initial measurements on the system were made with the capacitive probes. As shown in Figure 17, three distinct pulses are launched from the Gatling system. Each pulse has an approximate magnitude of 125 kV and has a large degree of noise associated with its signal, some of which may be attributed to the capacitive probe differentiating the 15 ns pulse. Additional noise problems also lie in impedance mismatches of the system. For this purpose, the triggering of Marx C was intentionally delayed to illustrate noise levels.

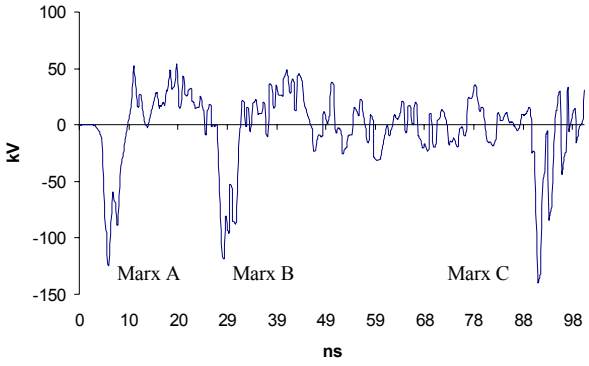

Figure 17. Output waveform of the Gatling system measured with a capacitive probe.

GENERATION OF HIGH POWER RF

Several antenna designs are pursued including a linear half TEM horn and a spiral antenna. The initial focus is to gain an understanding of pulsed high voltage antenna characteristics, and to establish antenna baseline parameters for gain, radiation pattern, optimal impedance transformation requirements, and field polarization over the frequencies of interest. Future designs will build on these results.

HIGH VOLTAGE ANTENNAS FOR DIRECT RF GENERATION

The linear half TEM-styled horn antenna is illustrated in Figure 18. This antenna is characterized by a single TEM plane extending over a large ground plane. The TEM plane linearly expands in both the E and H directions as the wave propagates toward the output. As a result, the characteristic impedance should linearly expand from the 50 Ω input impedance to the 377 Ω characteristic impedance of free space.

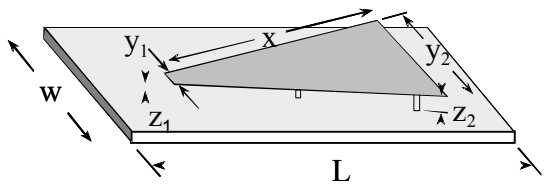

Figure 18. Geometry of the linear half TEM horn antenna.

The basic transmission line equation for a parallel plate line is used for the design; however, since the antenna transitions from the RG-220 coaxial cable and is to be operated at very high voltages, the input portion of the antenna has an insulator other than air. As the wave propagates toward the output, the insulator

tapers to a zero thickness. Thus, at the input, the width of the TEM plate is defined as

$$w = h\frac{377}{Z_o\,\varepsilon_r^{1/2} - 2} \qquad (1)$$

This dimension determines the high frequency cutoff for the antenna. However, the additional parameter of high voltage hold-off must be considered. While a small plate separation may allow for the radiation of higher frequency terms, failure of the antenna may result from too little insulating material.

The characteristic impedance of the output end of the TEM plate is defined by

$$w = h\frac{377}{Z_o\,\varepsilon_r^{1/2}} \qquad (2)$$

This dimension is chosen to match the impedance of free space and also defines the low frequency cut-off of the antenna.

Ideally, the linear half-TEM antenna should have a frequency response ranging from 3 GHz down to less than 100 MHz. However, the high voltage concerns, coupled with the desire to maintain compactness seems to dictate the final design. The input connection is designed for easy connection to the RG-220 cable. The cable connection is orthogonal to the wave propagation; however, the insulating material of the feed connection continues between the plates in the direction of the wave propagation to minimize premature breakdown. A frequency spectrum of more than 2 GHz to 500 MHz is chosen, maintaining some degree of compactness.

Design of the input plate separation begins with the high frequency cut-off point. In the case of the experimental Marx generator, this is 214 mm, which would result in a large reflection point. However, the insulating material of RG-220 is approximately 8.5 mm. Therefore, a plate separation of 8 mm is chosen to minimize unwanted reflects while maintaining high frequency content. Also note that using acrylic for the insulating material, a theoretical 125 kV can be applied before breakdown occurs. Using equation (1), the plate width is derived to be approximately 40 mm.

The plate separation at the output is chosen at a nominal 290 mm. The width of the plate is derived from equation (2). The following dimensions, as defined by Figure 17 result.

w = 600 mm L = 1220 mm

x = 910 mm

y1 = 40 mm y2 = 290 mm

z1 = 8 mm z2 = 290 mm

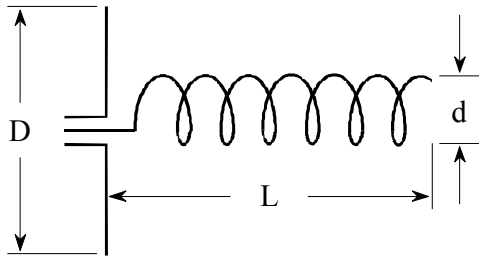

Figure 19. The spiral antenna.

Spiral antennas offer more control over the radiated frequency. These antennas offer bandwidths of 2:1, and up to 5:1 are possible. They are unidirectional and are circularly polarized. As illustrated in Figure 19, once the center conductor parts from the ground plane, it spirals around an imaginary cylinder whose circumference is approximately one wavelength in diameter. Choosing the number of coils, which defines the gain, the length, L is derived from a coil spacing definition of $\lambda \sin\theta$, where θ is typically 12 – 14 degrees. The minimum ground plane diameter is ¾ λ.

The spiral antenna, like the half-TEM ground plane antenna, is fabricated for easy connection with the RG-220 cable. The antenna is designed for an operating frequency of 1 GHz and 10 turns. Therefore, the coil diameter, d, is set at 95 mm, with a length, L, of 770 mm. The ground plane diameter. D, is chosen at 230 mm.

TEST RANGE

The antennas are range tested in an open field with a configuration illustrated in Figure 20. The antennas are separated by 100 m and elevated to a height of 10 m to delay the effects of ground bounce for approximately 7 ns. A receiving probe was purchased from Farr Research [5] (model number FRI-TEM-2-50) and feeds a Tektronix TDS 694C oscilloscope (3 GHz, 10 GS/s).

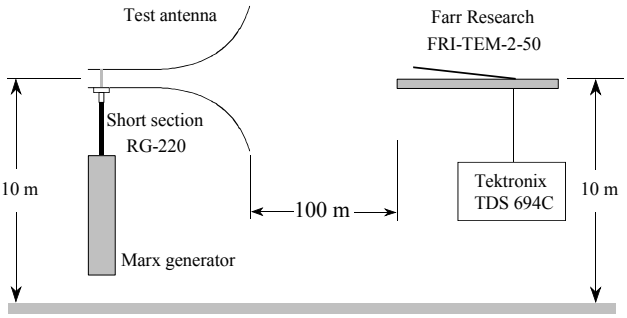

Figure 20. Test range illustration.

ANTENNA MEASUREMENTS

The linear half-TEM horn antenna is driven by the experimental Marx generator, resulting in the measured waveform shown in Figure 21. An approximate monopulse results with an electric field of approximately 1100 V/m at 100 m. The pulse is characterized by the Marx generator's 250 ps rise time and has an impulse width of less than 300 ps, FWHM. Also note in Figure 21 the ground bounce signal following 7 ns from the original signal.

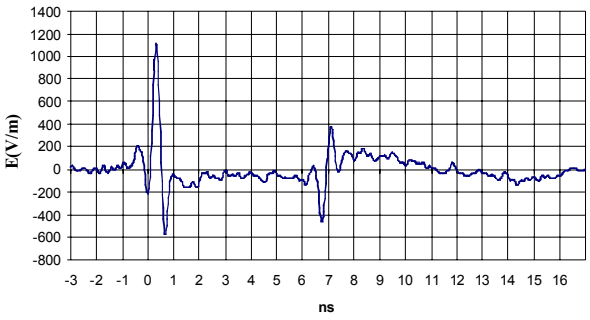

Figure 21. Radiated signal from the linear half TEM.

The Fourier spectrum resulting from the monopulse waveform is shown in Figure 22. As expected, the majority of the signal energy resides in the lower frequencies, from approximately 1 GHz down through 100 MHz. Not realized in this depiction is the energy lost, or attenuated by the antenna, since the low frequency cut-off is approximately 500 MHz. Future efforts will quantify the energy lost, as well as analyzing the trade-off between attenuation and the geometry compactness that lead to the design of a smaller antenna.

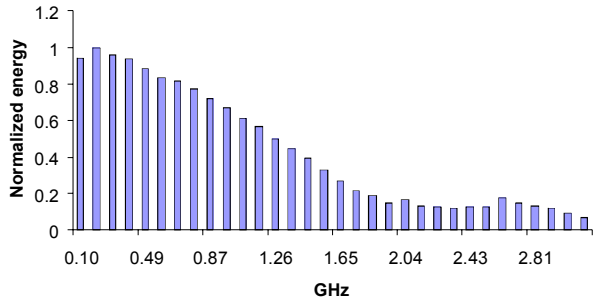

Figure 22. The normalized FFT of the linear half-TEM.

To gain some knowledge of the antennas performance beyond field strength measurements, simple Time Domain Reflectometry (TDR) measurements are made. As shown in Figure 23, a Tektronix 11801C sampling oscilloscope with an SD-24 module is used for the TDR measurement. A 2 m section of RG-220 is fitted with an SMA connector for connection to the oscilloscope, while the opposite end fits the customized antenna interconnection.

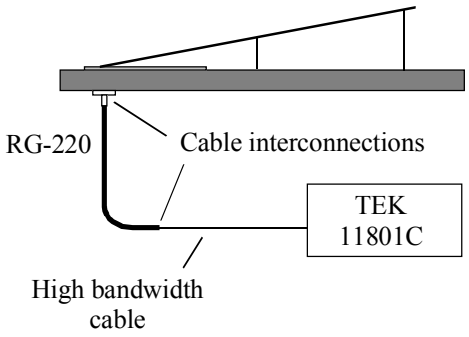

Figure 23. TDR measurement configuration.

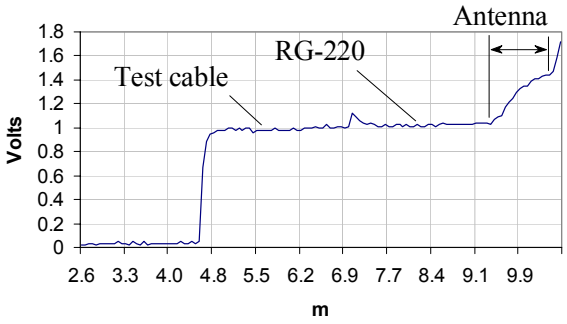

Figure 24. The TDR measurement of the linear half TEM.

The TDR measurement for the linear half TEM horn is shown in Figure 24. The TDR trace shows the somewhat linear impedance gradient of the antenna. The points of interest include the RG-220 cable, the interconnection between the antenna and the RG-220, the insulator at the input of the cable as well as the TEM plate itself. The RG-220 appears to be somewhat noisy, varying in impedance by several Ohms as the wave propagates the cable. The interconnection between the RG-220 and the antenna appears inductive, as anticipated, due to the orthogonal transition. The transition from the acrylic spacer is apparent and should be made more gradual in future designs.

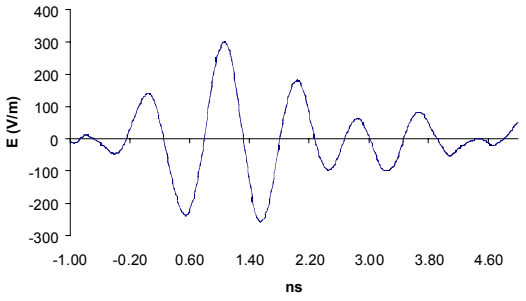

Figure 25. Radiated signal from the 1 GHz coil.

Figure 25 provides the measured radiation waveform of the coil antenna sourced by the Marx generator. As shown, several cycles of energy are delivered at approximately 1 GHz. Both vertical and horizontal polarization measurements were made, with each revealing an electric field of approximately 300 V/m at 100 m. Figure 26 provides the normalized Fourier spectrum, revealing that a narrow band of energy was radiated.

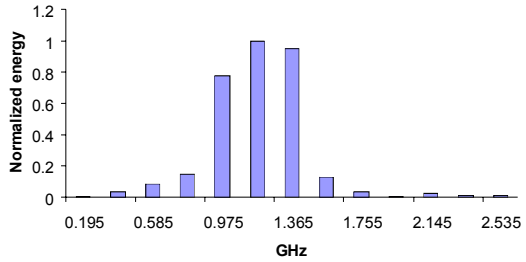

Figure 26. The normalized FFT of the 1 GHz coil.

The TDR measurement results of the 1 GHz coil antenna are shown in Figure 27. In this case, the transition from the RG-220 and the antenna is more uniform, likely due to the fact that the coil's conductor is very similar in size and shape to that of the RG-220's center conductor. The TDR results also seem to indicate that the impedance gradient from 50 Ω to 377 Ω is quick. Also noted is the rate change in the impedance that appears between the first and second coil. Future efforts will work toward correlating the rate of change in the impedance to the measured field strength.

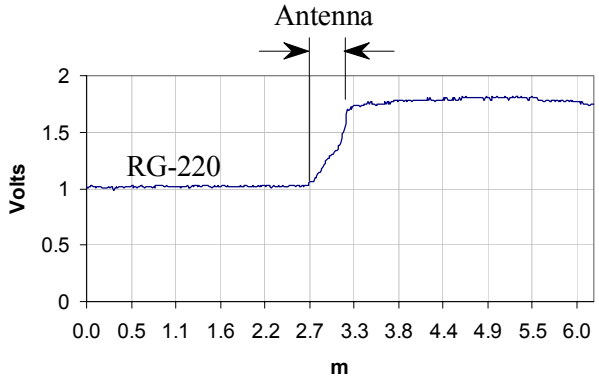

Figure 27. The TDR measurement of the 1 GHz coil.

GENERATION OF HIGH POWER MICROWAVE

The narrowband Marx generator was designed to drive the cathode of a Russian-made BWO in a collaborative effort with Texas Tech University[6]. As shown in Figure 28, the Marx generator directly drove the cathode and was temporally aligned with the magnetic field pulse. An uncalibrated, integrated B-dot probe was used to monitor the generated signal, as well as a fluorescent witness plate.

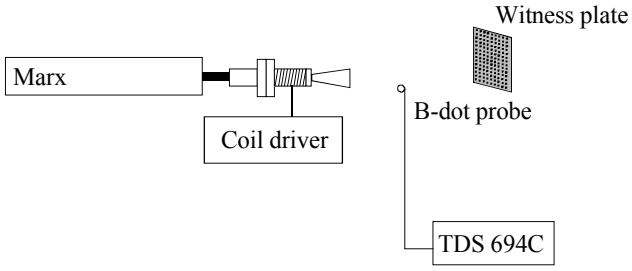

Figure 28. Experimental arrangement for the BWO System.

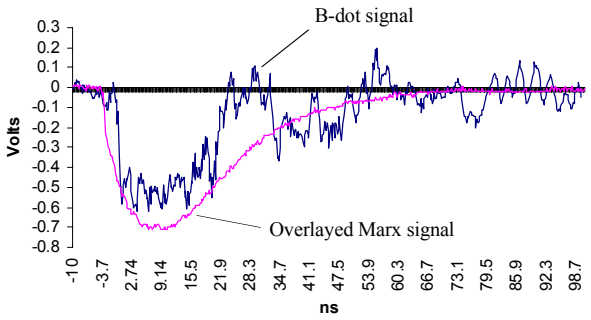

Figure 29. Results from the BWO testing.

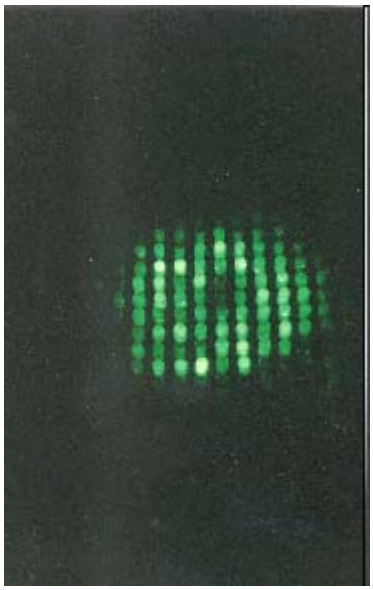

Figure 30. Fluorescent plate results of the BWO radiation.

The BWO was designed to deliver a 35 GHz signal within a 3 – 4 ns envelope. As shown in Figure 29, the system appears to deliver a 20 ns window of microwave energy that was approximated to be 30 MW in peak power. As illustrated in the photograph of Figure 30, the BWO delivered a TM01 mode.

CONCLUSION

This paper has presented the efforts made by Applied Physical Electronics, L.C. over the last several years to develop compact pulsed power sources for the generation of RF and HPM. To date, two generators have been developed, the impulse generator and the moderate pulse generator. With an emphasis on the impulse generator, efforts have been focused toward maximizing the voltage impulse efficiency while minimizing the system's volume. Further efforts have been made toward reducing the temporal jitter aimed at making the generator a viable radar source.

Initial demonstrations with the APELC generators for RF generation have proven to be very successful. Using an un-modified impulse generator, UWB and narrowband antennas have been directly connected to the generator and driven to produce high field strength RF, and thus demonstrating the direct generation of RF energy.

Future efforts will continue the development of these generators as well as the candidate antennas, with the primary goal of delivering compact pulse power systems capable of delivering very intense RF energy in both the UWB and narrowband realms.

REFERENCES

1. J. R. Mayes and W. J. Carey, *The Marx Generator As An Ultra Wideband Source*, 13th IEEE International Pulsed Power Conference, Las Vegas, NV, July 2001.
2. *The Gatling Marx Generator System*, J.R. Mayes and W.J. Carey, International Pulsed Power Conference, 2001.
3. G. Schaefer, Gas Discharge Closing Switches, Plenum Press, New York, 1990.
4. J.R. Mayes, *The Injection Wave Generator, Dissertation*, The University of Missouri-Columbia, 1998.
5. Farr Research, 614 Paseo Del Mar NE, Albuquerque, NM 87123.
6. M. Kristiansen, Texas Tech University, Lubbock, Texas 79410.

CONTACT

Jon R. Mayes
Applied Physical Electronics, L.C.
P.O. Box 341149
Austin, Texas 78734
(512) 264-1804
mayes@apelc.com